VHCF response of Gaussian SLM AlSi10Mg specimens: Effect of a stress relief heat treatment

VHCF response of Gaussian SLM AlSi10Mg specimens: Effect of a stress relief heat treatment

Authors:
A. Tridello[a], J. Fiocchi[b], C.A. Biffi[c], G. Chiandussi[d], M. Rossetto[e], A. Tuissi[f], D.S. Paolino[g]

[a] Department of Mechanical and Aerospace Engineering, Politecnico di Torino, 10129 Turin, Italy, andrea.tridello@polito.it
[b] CNR ICMATE – Institute of Condensed Matter Chemistry and Technologies for Energy, 23900 Lecco, Italy, jacopo.fiocchi@icmate.cnr.it
[c] CNR ICMATE – Institute of Condensed Matter Chemistry and Technologies for Energy, 23900 Lecco, Italy, carloalberto.biffi@cnr.it
[d] Department of Mechanical and Aerospace Engineering, Politecnico di Torino, 10129 Turin, Italy, giorgio.chiandussi@polito.it
[e] Department of Mechanical and Aerospace Engineering, Politecnico di Torino, 10129 Turin, Italy, massimo.rossetto@polito.it
[f] CNR ICMATE – Institute of Condensed Matter Chemistry and Technologies for Energy, 23900 Lecco, Italy, ausonio.tuissi@cnr.it
[g] Department of Mechanical and Aerospace Engineering, Politecnico di Torino, 10129 Turin, Italy, davide.paolino@polito.it

Corresponding Author:
A. Tridello
E-mail address: andrea.tridello@polito.it
Full postal address:
C.so Duca degli Abruzzi 24,
Department of Mechanical and Aerospace Engineering – Politecnico di Torino,
10129 – Turin,
ITALY
Phone number: +39.011.090.6913
Fax number: +39.011.090.6999

Abstract:

The present paper investigates the effect of a stress relief heat treatment (two hours at 320 °C and air cooling down) on the VHCF response of an AlSi10Mg alloy produced through SLM. Ultrasonic tension-compression tests up to 10^9 cycles were carried out on as-built and heat treated Gaussian specimens with a large loaded volume. Experimental results showed that the investigated heat treatment has a detrimental effect on the VHCF response: VHCF strength reduction is larger than 20% at number of cycles above 10^8 The microstructural changes induced by the heat treatment (i.e., rupture and spheroidization of the original eutectic silicon network) was shown to be the main reason for the VHCF decrement, thus suggesting that an optimization of the heat treatment parameters is required.

Keywords: Additive Manufacturing; Selective Laser Melting (SLM); Very High Cycle Fatigue (VHCF); AlSi10Mg alloy; heat treatment.

Acronyms and nomenclature

AM: Additive Manufacturing

SLM: Selective Laser Melting

VHCF: Very High Cycle Fatigue

AB sample: as-built sample

HT sample: heat treated sample

σ_s: yield stress

σ_u: ultimate tensile strength

ε_f: elongation to failure

HV: Vickers hardness

Ra: surface roughness

s_{spec}: stress amplitude measured by the gage bonded at the center of the Gaussian specimen (calibration gage)

s_{horn}: stress amplitude measured by the gage bonded to the horn (control gage)

s_{local}: local stress amplitude, stress amplitude at the defect location.

SIF: Stress Intensity Factor

$\sqrt{a_c}$: square root of the projected area of the defect originating failure (critical defect)

K_{th}: SIF threshold

rv: random variable

μ, σ_Y: mean and standard deviation of the fatigue life rv.

c_Y, m_Y, n_Y: constant coefficients

N_f: the number of cycles to failure

Z: standardized Normal rv

n_{ref}: reference number of cycles

S_{corr}: VHCF strength at the reference number of cycles

$F_{S_{corr}}$: cumulative distribution function of the S_{corr} rv

$\mu_{S_{corr}}$, $\sigma_{S_{corr}}$: mean and standard deviation of the S_{corr} rv

1. INTRODUCTION

In the last decades, the use of Additive Manufacturing (AM) techniques for the production of metallic components used in structural applications has rapidly increased. Among the AM techniques, Selective Laser Melting (SLM) is particularly widespread, especially for aluminum alloy processing. SLM permits to manufacture parts characterized by very good quasi-static mechanical properties [1] that can even outperform those of parts manufactured with traditional subtractive technologies. Nonetheless, the fatigue loads are critical: defects originating during the building process, such as pores induced by vaporization of light elements, incomplete melting of powder and residual oxide layers, may significantly affect the fatigue response of SLM parts [2-5]. Therefore, a proper experimental characterization of the fatigue behavior of AM components is mandatory to ensure a safe and conservative fatigue design. In the literature, many researches [2-5] have carried out to assess the High Cycle Fatigue (HCF) behavior of SLM parts; on the other hand, the Very-High-Cycle Fatigue (VHCF) response of these parts has been rarely investigated [6-9]. In particular, in Reference [6] the VHCF response of Ti6Al4V parts was investigated, focusing on the effect of the stress ratio and of different post process treatment, (i.e., the stress relief heat treatment and the Hot Isostatic Pressing, HIP). In [7], the VHCF behaviour of SLM AlSi12 specimens was assessed, focusing mainly on the crack propagation process from defects originating during the AM process. In [8], the VHCF of Ti6Al4V hourglass specimens obtained through SLM and EBM was compared, with particular attention dedicated to the defects originated during the manufacturing process. In [9], the VHCF response of as-built AlSi10Mg specimens was investigated and the defect population in large loaded volumes was statistically assessed. However, to further extend the use of AM parts to structural applications, such as turbine palettes and automotive engine components, subjected to critical high frequency loads and to VHCF loads, the VHCF response must be properly experimentally investigated..

As for components produced through traditional processes, many different factors affect the fatigue response of AM parts: among the others, manufacturing process parameters such as as specimen orientation with respect to the building direction, heating of the building platform, surface roughness [10], defects size distribution [5] and residual stresses [11], have a significant influence on the fatigue response. Even heat treatments could affect the fatigue response [2, 12]. The effect of traditional heat treatments, usually applied

to cast components, has been investigated in the literature (see e.g. the study carried out in [2]). Moreover, many different heat treatments that are specifically for SLM parts are being proposed by producers. The effect on the HCF and the VHCF response is still under investigation and of utmost interest among researchers and industry.

In the present paper, ultrasonic VHCF tests on AlSi10Mg specimens produced through SLM were carried out. Experimental tests were performed on as-built specimens and on specimens subjected to a heat treatment for stress relief, which was recommended by the AM machine manufacturers for SLM parts. It induced a decrement of the material's tensile strength and hardness, while significantly increasing ductility. Tension-compression ultrasonic tests up to 10^9 cycles at a loading frequency of 20 kHz at were performed by using the ultrasonic testing machine developed at the Politecnico di Torino [13]. To study the size-effect in VHCF [14-16], Gaussian specimens with large loaded volumes [16-19] of 2300 mm^3 were used for the ultrasonic tests. According to the dependence between the defect size and the loaded volume (the larger the loaded volume, the larger the probability of large and critical defects), tests on large loaded volumes allow for a more conservative estimation of the VHCF response. The VHCF response of components is generally estimated from experimental results obtained through tests on small hourglass specimens. However, according to [20], dangerous non-conservative prediction of the VHCF response may be obtained with tests on small loaded volumes, since the distribution of the defect size cannot be properly estimated. On the contrary, Gaussian specimens permit to increase the attainable loaded volume. The specimen profile is described by a Gaussian function [16, 21] which ensures a uniform stress distribution and permits to test loaded volumes significantly larger than those of hourglass and dog-bone specimens and, therefore, to obtain a safer and more conservative estimation of the VHCF response. Fracture surfaces were investigated with a Scanning Electron Microscope (SEM) to assess the failure origin. The defect populations, the Stress Intensity Factor thresholds and the VHCF strengths were finally statistically analyzed.

2. MATERIALS AND METHODS

The present section describes the experimental activity in detail: Subsection 2.1 concerns the material properties, the SLM process parameters and describes the applied heat treatment and the experimental

setup of the quasi-static mechanical tests.. Subsection 2.2 describes the ultrasonic testing machine used for the VHCF tests. In the following, AB specimens will refer to as-built specimens, whereas HT specimens will refer to heat treated specimens.

2.1. Materials and SLM process parameters

Spherical gas atomized AlSi10Mg powders (i.e. the EN AC 43000 alloy), whose nominal chemical composition is reported in Table 1, were used as SLM starting material. The particles size follows a Gaussian distribution in the range 20–63 μm, with average size of approximately 45 μm, 10 % of particles below 28 μm and 10 % above 70 μm.

Si	Mg	Cu	Ni	Fe	Mn	Ti	Al
10	0.4	< 0.25	< 0.05	< 0.25	< 0.1	< 0.15	bal.

Table 1: Chemical composition of the AlSi10Mg powder (wt. %) [22]

A SLM Solutions (model 500 HL quad 4 × 400 W) Selective Laser Melting system, equipped with 4 continuous wave fiber lasers having maximum power of 400W, was used to manufacture the samples for the experimental tests. All the samples were built with their symmetry axis lying in the x-y plane, i.e. in the plane which is scanned by the laser [23]. The platform temperature was heated to 150° C. Thin support structures were built beneath the central part of the specimens to support the building part. Table 2 reports the process parameters adopted for the production of the specimens. These parameters are those supplied by the SLM equipment producer and are optimized for an AlSi10Mg alloy. They were thus chosen to perform an industrially valuable study case.

Power	***Building plate temperature***	***Scanning speed***	***Spot size***	***Hatch distance***	***Layer thickness***	***Atmosphere***
350 W	150 °C	1.15 m/s	80 μm	170 μm	50 μm	Argon

Table 2: SLM process parameters used for building the AlSi10Mg specimens.

Ultrasonic tests were performed on as-built and on heat treated specimens. The heat treatment involved annealing for two hours at 320 °C and subsequently air cooling down to room temperature. The considered heat treatment, suggested by the AM system manufacturers [24, 25], was aimed at stress relieving and homogenizing the SLM – built parts.

The microstructure of the as-built and heat treated AlSi10Mg specimens was deeply investigated in [25-26] and is depicted in Fig. 1: the manufactured specimens show the typical as-built AM microstructure (Fig. 1 a), characterized by a columnar solidification structure that follows the shape of the localized melting pools originated by the manufacturing process. At a lower scale the supersaturated aluminum matrix appears decorated by a continuous network of eutectic silicon. On the other hand, the microstructure of the heat treated specimens (Fig. 1 b) is characterized by a fine distribution of Si particles, arising from the rupture and spheroidization of the original network. Fe-bearing secondary phases, which are known to detrimentally affect the mechanical behaviour, were not found neither in as-built nor in heat treated samples.

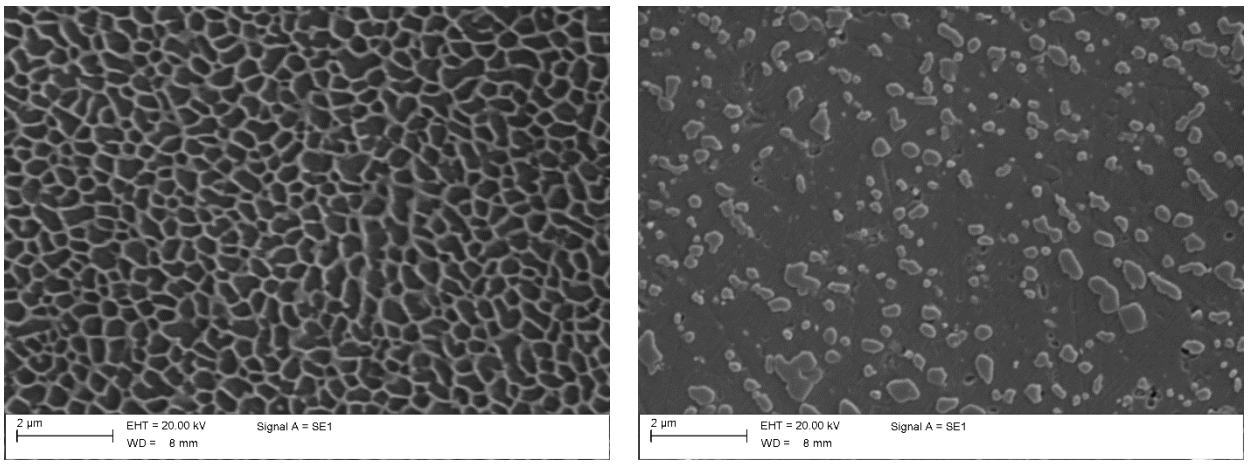

Figure 1: SEM micrographs of AB (a) and HT samples (b) along the x-y plane.

The effect of the heat treatment on the quasi-static mechanical properties, tensile strength and Vickers hardness, was experimentally assessed. Tensile tests were carried out according to ASTM E8/E8M-09 standard on three sub-size dog-bone specimens (produced by considering the process parameters reported in Table 2) by using a MTS 2/M machine (strain rate of $0.015\ \mathrm{min}^{-1}$), equipped with an extensometer. No machining was applied to the specimens before testing.

Vickers hardness was measured on the cross-section of four AB and four HT Gaussian specimens failed during the VHCF tests (Section 2.3) according to the ISO Standard [27]. Experimental results are compared in Section 3.1.

2.2. Ultrasonic testing configuration

Ultrasonic VHCF tests were carried out on Gaussian specimens [16-18] with a 90% risk-volume, V_{90}, equal to $2300\ \mathrm{mm}^3$. According to [14-15], the V_{90} is defined as the volume of material subjected to a stress amplitude larger than 90% of the maximum stress amplitude. Gaussian specimens permit to test risk-volumes significantly larger than those attainable with hourglass and dog-bone specimens commonly adopted in literature [28]. For design of AM parts, it is well known that defect size and population has great effect on fatigue performance [5]. These features must be accurately assessed. Since VHCF failures typically originate from the most critical defects present within the risk-volume, VHCF tests on Gaussian specimens can be effectively used for a reliable assessment of the population of critical defects as well as of their size distribution.

Gaussian specimens were finely manually polished before experimental tests by using sandpaper with increasing grit (from 240# to 1200#) in order to remove macroscopic superficial defects and residual support structures. The executed polishing process does not affect the defect population [5] and permits to remove large superficial scratches that would originate premature failures (invalid data according to Section 3.2); on the other hand, it significantly enhances the probability of failure from internal and sub-superficial defects, which are of interest for the present study. The surface roughness Ra of the tested specimens before and after the polishing process was measured on five specimens by using a Mitutoyo Surftest SV-500 instrument and was equal to $5.15\ \pm\ 0.38\ \mu\mathrm{m}$ and $1.41\ \pm\ 0.26\ \mu\mathrm{m}$, respectively.

Fig. 2 (a) shows the geometry of the Gaussian specimen; Fig. 2 (b) shows the Gaussian specimen after the polishing process.

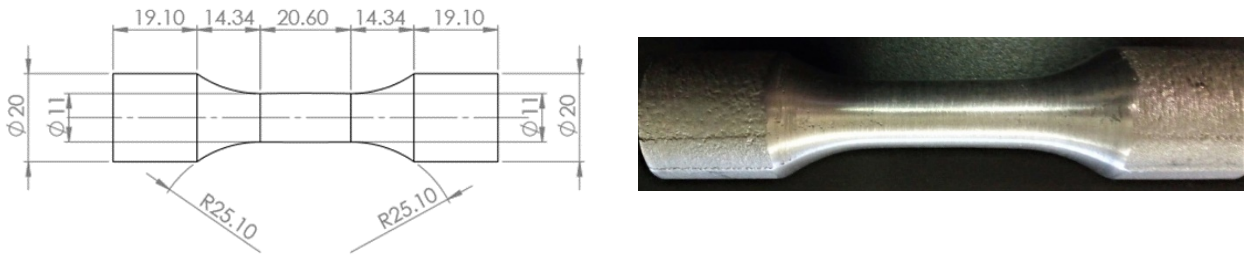

(a) (b)

Figure 2: Gaussian specimen used for the ultrasonic VHCF tests: (a) geometry of the Gaussian specimen; (b) Gaussian specimen after the polishing process.

Fully reversed tension-compression tests at constant stress amplitude were carried out up to failure or up to 10^9 cycles (runout specimens) by using the Ultrasonic Fatigue Testing Machines (UFTMs) developed at the Politecnico di Torino. The UFTM has the typical configuration of those described in the literature [29]. In particular, the UFTMs used for the experimental tests consist of: (1) an ultrasonic generator, Branson DCX 4 kW, that generates an electric sinusoidal signal with frequency of 20 kHz; (2) a piezoelectric transducer, that converts the electric signal in mechanical vibration; (3) two mechanical amplifiers (a booster and a horn), rigidly connected to the piezoelectric transducer; (4) the specimen that is rigidly connected to the horn through an adhesive joint [30] and is subjected to fully reversed tension-compression load. The piezoelectric transducer and the booster were provided by the Branson Ultrasonics Corporation. The horn was designed by the Author. The control system, which permits to monitor the main test parameters during the tests, such as the applied stress amplitude, the number of cycles and the specimen temperature, was developed by the Authors in a *LabView* environment.

The stress amplitude within the specimen risk-volume was kept constant through a closed loop control based on the strain amplitude measured by a strain gage (HBM 1-XY31-1.5/350) bonded to the horn (*control gage*). The correlation between the strain amplitude within the risk-volume and the strain measured by the *control gage* was verified by bonding a second strain gage (*calibration gage*) at the center of the Gaussian specimen.

Fig. 3 shows the horn and the specimen after the application of the *control gage* and of the *calibration gage*.

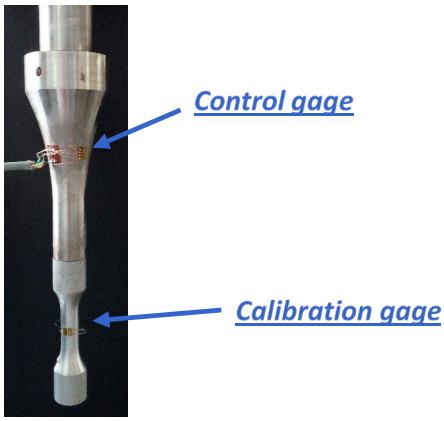

Fig. 3: Horn and specimen after the application of the *control gage* and of the *calibration gage*.

Fig. 4shows the stress amplitude measured by the *calibration gage*, s_{spec}, with respect to the stress amplitude measured by the *control gage*, s_{horn}. The two stresses, s_{spec} and s_{horn}, were obtained from the measured strain amplitude and by considering the average Dynamic Young modulus experimentally measured by using the Impulse Excitation Technique (IET). The calibration procedure was performed on three AB and on two HT specimens, at four increasing voltage amplitudes imposed by the piezoelectric transducer.

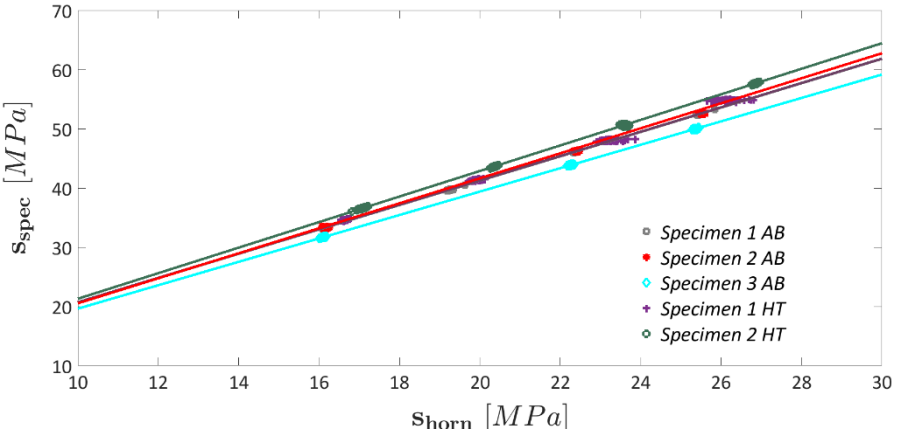

Figure 4: Stress amplitude measured by the *calibration gage*, s_{spec}, with respect to the stress amplitude measured by the *control gage*, s_{horn}.

According to Fig. 4, for the same measured s_{horn}, the variation of s_{spec} among the three AB and the two HT tested specimens was limited, thus confirming that the control system based on s_{horn} is effective and reliable. For the specimens not used for the calibration, an average calibration curve was considered for correlating s_{spec} and s_{horn}. For the range of the applied stress amplitude, the maximum uncertainty on the applied stress was smaller than $\pm$ 1.5 MPa and $\pm$ 1 MPa for AB and HT specimens, respectively. The limited range of uncertainty confirms that the SLM Gaussian specimens can be reliably tested and that the stress

amplitude can be controlled with high accuracy, notwithstanding the large manufacturing tolerances typical of AM parts. Moreover, in order to verify the effectiveness of the control system, a *load histogram* was recorded during each test to verify the percentage of the total number of cycles performed at the imposed stress amplitude. The load histogram confirms that the control system permits to effectively keep the stress amplitude constant during the test, with more than 99% of the total number of cycles in the range $\pm$ 1 MPa. Specimen self-heating [31] was also taken under control during the experimental tests. In particular, the temperature at the specimen center was continuously monitored during the tests with an infrared temperature sensor (OPTRIS CT-LT-15) and it was always kept below 298 K by using three vortex tubes. The temperature uniformity within the risk-volume of Gaussian specimens was also verified in [32].

3. EXPERIMENTAL RESULTS

In Section 3 the experimental results are presented and analyzed. Subsection 3.1 and Subsection 3.2 report the results of the quasi-static tests and the results of the ultrasonic VHCF tests, respectively. In Subsection 3.3 fracture surfaces are investigated. In Subsection 3.4 and Subsection 3.5 the Stress Intensity Factor (SIF) threshold and the VHCF strength are compared. Finally, in Subsection 3.6 the experimental results and the effect of the heat treatment on the VHCF response are discussed.

3.1. Quasi-static mechanical properties: experimental results

In this Section the results of the quasi-static mechanical tests are analyzed. Fig. 5 shows the Average stress-strain curves for the as-built and the heat treated AlSi10Mg specimens.

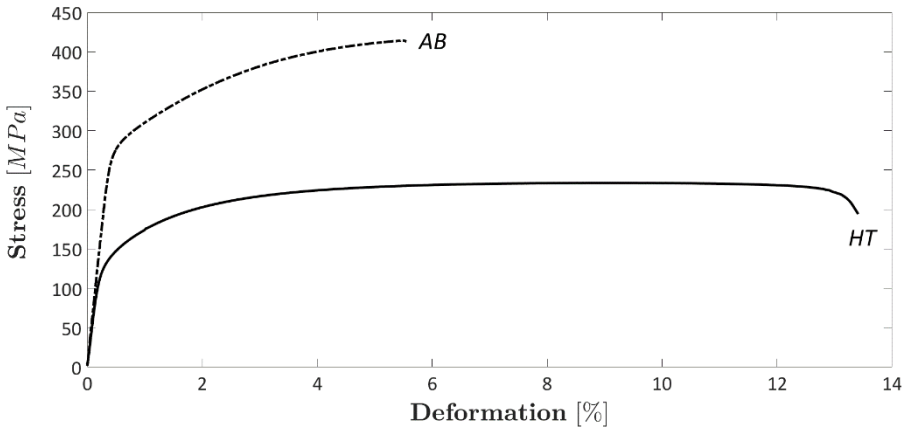

Figure 5: average stress-strain curves for the as-built and the heat treated AlSi10Mg specimens.

According to Fig. 5, the tensile strength, σ_u, reduced significantly after the heat treatment, being almost the half of that measured in AB specimens. On the other hand, the ductility significantly increases: the elongation to failure (ε_f) after the heat treatment is about 2.4 times larger than that measured in AB specimens. Table 3 compares the measured quasi-static mechanical properties (yield stress, σ_s, ultimate tensile strength, σ_u, and elongation to failure, ε_f). The present values are consistent with those reported in literature for SLM-built AlSi10Mg parts, both in the as-built and annealed conditions [33]. When comparing the performance of SLM parts to that of die cast samples [34], it must be pointed out that the as-built specimens exhibit better mechanical properties in terms of both σ_s (175 MPa) and σ_u (320 MPa). On the other hand the heat treated SLM parts show lower strength but much larger ε_f (3 %) thanks to the more uniform microstructure and to the absence of enbrittling phases such as the Fe-bearing ones [35].

	$\boldsymbol{\sigma_s}$ **[MPa]**	$\boldsymbol{\sigma_u}$ **[MPa]**	$\boldsymbol{\varepsilon_f}$ [%]
As-built	$287\ (\pm 5)$	$413\ (\pm 7)$	$5.5\ (\pm 0.1)$
Heat treated	$142\ (\pm 5)$	$234\ (\pm 7)$	$13.4\ (\pm 0.1)$

Table 3: Quasi-static mechanical properties of AB and HT specimens.

Fig. 6 shows the Vickers hardness variation within the specimen cross-section for the selected AB (Fig. 6 a) and HT (Fig. 6 b) specimens. Vickers hardness was measured at the center of the cross-section and at two different locations, radius and half radius, along the positive and the negative x and y directions.

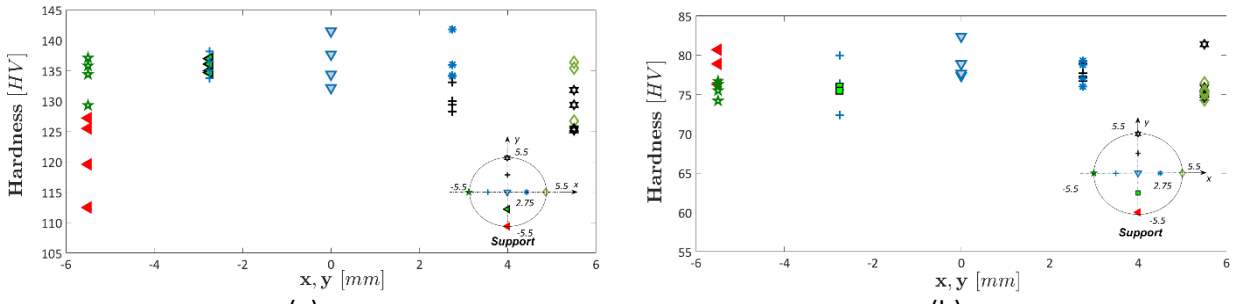

(a) (b)

Figure 6: Distribution of Vickers hardness within the specimen cross-section: a) AB specimens; b) HT specimens.

According to Fig. 6, the average Vickers hardness in AB specimens is equal to 134 HV and is almost constant within the cross-section. A small reduction of about 10% in the region where the support structures were mechanically removed can be observed: the HV reduction was computed as the difference between the average HV within the specimen section, HV_{mean} (without considering HV in the support region) and the average HV in the support region (HV_{sup}), divided by HV_{mean}. The hardness reduction in the support area is related to the heat accumulation caused by the presence of powder underneath the sample during the building process. In fact, it has been demonstrated in the literature [36] that, if compared to bulk metal, loose powder acts as barrier to heat conduction and thus induces a sort of thermal treatment in the layers, which are built immediately above it. The larger scatter in this area may be caused by the different thermal history experienced by parts built over support structures or over loose powder. After the heat treatment, the Vickers hardness significantly decreased, with an average value of 76 HV and a 42% variation. The scatter is reduced, with a maximum variation within the cross-section less than 7.5%. The overall reduction of mechanical resistance in heat treated samples, as revealed by both tensile and hardness tests, was mainly due to the coarsening of microstructure and the rupture of the fine Si network, typical of as-built SLM parts. For the same reasons ductility was strongly improved in annealed samples. Moreover, reinforcing precipitates such as the coherent β'' phase become coarsened and lose coherency upon prolonged holding at high temperature, thus becoming less efficient in obtruding dislocation motion.

3.2. Experimental dataset

Ultrasonic tests were carried out at nominal stress amplitudes (i.e., measured at the center of the specimen) between 60 MPa and 95 MPa. 9 out of 17 AB specimens failed in the range between $6.85 \cdot 10^4$ and $9.79 \cdot 10^9$, whereas 6 AB specimens did not fail at 10^9 cycles (runout specimens). 5 out of 8 HT specimens failed in the range between $4.92 \cdot 10^4$ and $2.53 \cdot 10^8$ and 2 runout specimens did not fail at 10^9 cycles. 3 specimens (2 for AB and 1 for HT) failed before 10^4 cycles due to large surface scratches in the area where support structures were removed and were not considered for the analysis.

All the fatigue failures, observed with an optical microscope and a Scanning Electron Microscope, SEM (LEO 1413), originated from surface or subsurface defects. The stress amplitude close to the defect location,

s_{local},which was assessed through Finite Element Analysis FEA by considering the exact location of each defect, was used for the analysis of the experimental data. Defect locations along the axial and the radial directions were measured with a digital caliper (resolution of 0.01 mm) and through digital image processing of the fracture surface, respectively. Fig. 7 shows the S-N plot of the experimental dataset, obtained by considering s_{local}.

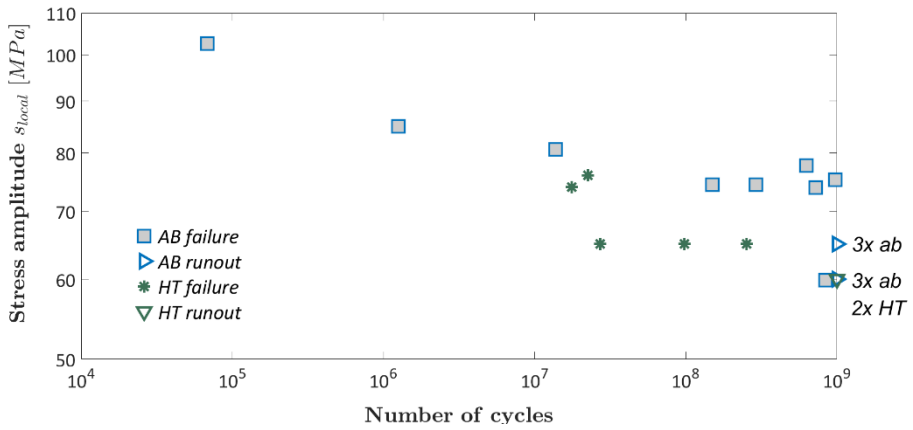

Figure 7: S-N plot of the experimental data obtained by considering s_{local}.

As shown in Fig. 7, the heat treatment is detrimental for the VHCF response: apart from one data, AB specimens exhibit larger VHCF strength and life than HT specimens. The effect of the applied HT on the VHCF strength of the tested AlSi10Mg alloy will be investigated in a statistical framework in Section 3.4.

3.3. Defect analysis

The defects originating failure, referred to as critical defects in the following, are analyzed in detail in this Subsection. As expected, the fine polishing process enhances the probability of failures from defects within the material and only 3 out of 15 specimens failed due to large surface defects that were not eliminated with the polishing process. In agreement with [5], all the fatigue failures, both in AB and in HT specimens, originated from defects concentrated near the surface, with a maximum distance from the free surface equal to 275 μm in AB specimens and to 63 μm in HT specimens. According to [14], defects close to the surface are more critical: the SIF associated to surface and sub-surface defects is larger than the SIF of internal defects.. It is worth to note that a larger layer of superficial material should be removed, for instance through a machining process, to investigate the role of more internal defects.

Three types of defects, i.e. pores, surface and single subsurface, were classified in AB samples [9]: the single surface defect originated during the mechanical removal of support structures, whereas the single sub-surface defect originated due to an incomplete fusion of the powder during the building process and the Energy dispersive X-ray spectroscopy (EDX) technique confirmed that it is not an oxide-type defect. For HT specimens, typical single pore, clusters of pores and single surface defects were experimentally found and shown in Fig. 8 (a), (b) and (c), respectively. As for AB defects, single surface defects probably originated during the mechanical removal of the support structures. According to [14, 26], a group of defects close to each other was considered a cluster of defects if the distance between pores is smaller than the smallest pore of the group, Fig. 8 (b).

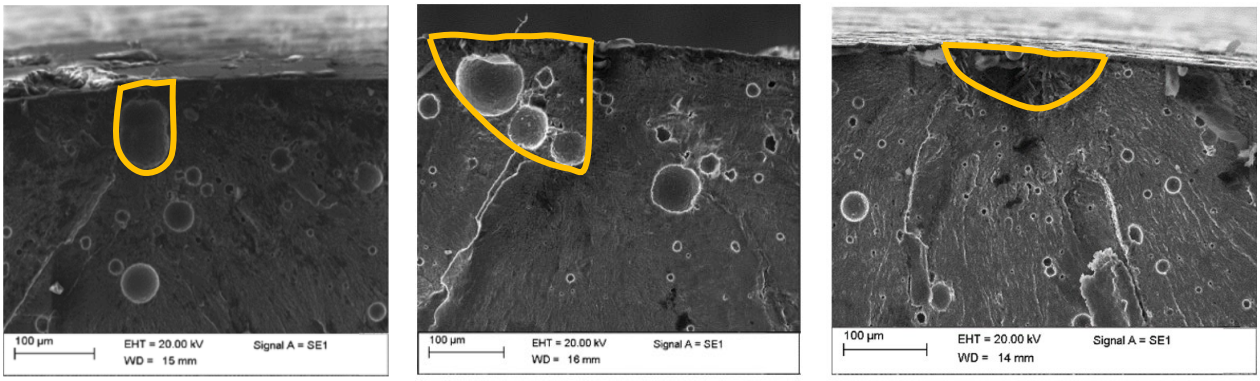

(a) (b) (c)

Figure 8: Defects originating failure in HT specimens: (a) single pore (HT); (b) cluster of pores (HT); (c) single surface defect, originating during the removal of supports (HT);

Pores were at the origin of the fatigue failures in 6 out of 9 failures (67%) for AB and in 4 out of 5 failures (80%) for HT. Surface defects originating during the mechanical removal of support structures and incomplete fusions were less frequent: the former initiated the fatigue crack in 2 out of 9 failures (22%) for AB and in 1 out 5 failures (20%) for HT, the latter in 1 out of 9 failures (11%) for AB. Therefore, pores were the most critical and the most frequent defect before and after the heat treatment.

The size of critical defects, $\sqrt{a_c}$, was also analyzed. Table 4 shows the size of defects originating failure. Defects originating during the AM processes are characterized by an irregular morphology and shape. In order to take into account the influence of the defect morphology, according to [14, 37], an equivalent defect

size, corresponding the real size of the defect involved in the crack nucleation process, should be considered, since it allows for a proper comparison of the influence of the defect on the fatigue response.

For each defect type, the smallest ($\sqrt{a_{c,min}}$) and the largest ($\sqrt{a_{c,max}}$) defect found experimentally are reported.

	$\sqrt{a_{c,min}}$ [μm]	$\sqrt{a_{c,max}}$ [μm]
All defects		
AB	103	198
HT	86	160
Pores		
AB	103	174
HB	86	160
Surface irregular defect		
AB	116	198
HT	102	102
Incomplete fusion defect		
AB	195	195
HT	/	/

Table 4: Size of the defects originating failures in AB and HT specimens.

According to Table 4, critical defects in AB specimens are larger ($[103 : 198]$ μm for AB and $[81: 160]$ μm for HT specimens). The $\sqrt{a_{c,max}}$ value in AB is about 19% larger than that in HT. Heat treatment seems to affect the defect size, if all the typologies of defects are taken into account. However, if only the spherical pores (or the equivalent size for cluster of pores) are considered, the dimension ranges of pores found in AB and HT samples do not significantly differ, being $[103: 174]$ μm for AB and $[86: 163]$ μm for HT. Therefore, the tested heat treatment does not significantly influence pore dimensions, in agreement with literature results [38-40] that show that a heating temperature of about 300° C does not alter the pore size. Moreover, experimental results reported in [41] show that heat treatments, in general, do not modify the pore size. By considering the other types of defects (defects originating during the mechanical removal of support structures and defects due to an incomplete fusion), they are larger in AB. However, a smaller number of HT

specimens was tested (9 failures in AB vs 5 in HT). For these types of defects, which occurred less frequently, the different size could be thus explained by considering the different sample size.

3.4. Stress Intensity Factor Threshold

According to [5], the large scatter of AM fatigue results is directly related to the scatter of the SIF threshold that, for short cracks (i.e., for $\sqrt{a_c} < 1000$ μm), strongly depends on the random distribution of the critical defect size. Indeed, as highlighted in [5], models for the analysis of AM fatigue results must necessarily take into account the defect size and, indeed, if $\sqrt{a_c}$ can be accurately estimated or experimentally assessed, the SIF threshold can be safely employed for the design of components [5,42]. The SIF threshold values are therefore analyzed in this Subsection.

According to [42], the SIF associated to the defect originating the fatigue failure, K_d, is equal to the K_{th} value for specimens failed below the so-called "knee point" (i.e., above the knee point, the crack starts propagating form the defect with a K_d larger than the K_{th}). In [42], the knee point is assumed to be equal to $2 \cdot 10^5$. In the following analysis only failures occurring at a number of cycles larger than $2 \cdot 10^6$ were therefore conservatively considered. For each failed specimen, K_d was estimated by considering the equivalent defect size, $\sqrt{a_c}$, and the defect location (surface or internal). Fig. 10 plots the K_{th} values with respect to $\sqrt{a_c}$ in a log-log scale for AB and HT specimens. Since AB and HT are characterized by different Vickers hardness, K_{th} values are normalized by the factor $(HV + 120)$ according to [14, 43]. A general linear mode [44] was considered for interpolating the experimental results: the median (thicker lines), the 0.05-th and the 0.95-th quantiles (dashed lines) of the K_{th} functions are shown in Fig. 9. The 0.05-th and the 0.95-th quantiles are estimated by considering K_{th} as normally distributed [44].

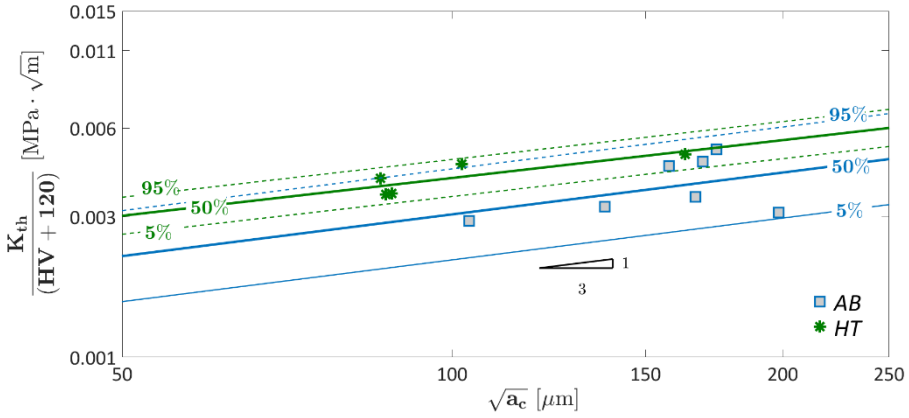

Figure 9: SIF threshold, K_{th}, with respect to the defect size $\sqrt{a_c}$.

According to Fig. 9, the linear model well describes the experimental results for both AB and HT specimens. Moreover, the slope of the two interpolating functions is about the same and is close to the values found in the literature ($[1/3 : 1/2]$, [5, 14]). Actually, the slope of the K_{th} function for the HT specimens is slightly higher. However, the interpolating function for HT is within the 80% confidence interval for AB. Therefore, it can be concluded that, for the investigated range of $\sqrt{a_c}$, the trend is the same and that the heat treatment has no effect on the K_{th} trend. It can also be noted that the scatter of the K_{th} values after the heat treatment is smaller: the standard deviation, equal to 0.11 for AB, reduces to 0.038 for HT. Residual stresses can be considered to justify the reduction of the experimental scatter, as will be discussed in Section 3.5.

3.5. VHCF strength at 10^8 cycles

To compare the VHCF strength of AB and HT specimens, the experimental failures were gathered together at a reference number of cycles to failure, n_{ref} [9, 45]. By considering the fatigue life as a Normal random variable (rv) with constant standard deviation and mean that linearly depends on the logarithms of the applied stress amplitude and of the defect size (i.e., $\log_{10}[N_f] = c_Y + m_Y \log[s_{local}] + n_Y \log_{10}[\sqrt{a_{d,0}}] + Z\sigma_Y$, being N_f the number of cycles to failure, c_Y, m_Y and n_Y constant coefficients, Z the standardized Normal random variable and σ_Y the standard deviation), it is possible to obtain, for each experimental failure, the corresponding VHCF strength, S_{corr}, at the reference number of cycles, n_{ref}. According to [9], S_{corr} is a Normal rv with mean equal to $\mu_{S_{corr}}$ ($\mu_{S_{corr}} = -\frac{c_Y}{m_Y} + \frac{\log_{10}[n_{ref}]}{m_Y} - \frac{n_Y}{m_Y}\log_{10}[\sqrt{a_{d,0}}]$) and standard deviation $\sigma_{S_{corr}}$ equal to $-\frac{\sigma_Y}{m_Y}$:

$$F_{S_{corr}} = \Phi\left[\frac{s_{corr}-\mu_{S_{corr}}}{\sigma_{S_{corr}}}\right]. \quad (1)$$

The constant coefficients c_Y, m_Y and n_Y have been estimated through a multiple linear regression, according to [44]. Fig. 10 a) and Fig. 10 b) show the probability density functions of S_{corr} ($f_{S_{corr}} = \frac{1}{\sigma_{S_{corr}}}\varphi\left[\frac{s_{corr}-\mu_{S_{corr}}}{\sigma_{S_{corr}}}\right]$) at $n_{ref} = 10^8$ cycles and at $n_{ref} = 2 \cdot 10^8$ cycles, respectively, for an initial defect size equal to 148 µm and corresponding to the median experimental value for $\sqrt{a_c}$. The n_{ref} values (10^8 and $2 \cdot 10^8$ cycles) were chosen within the range of the number of cycles to failure of HT specimens.

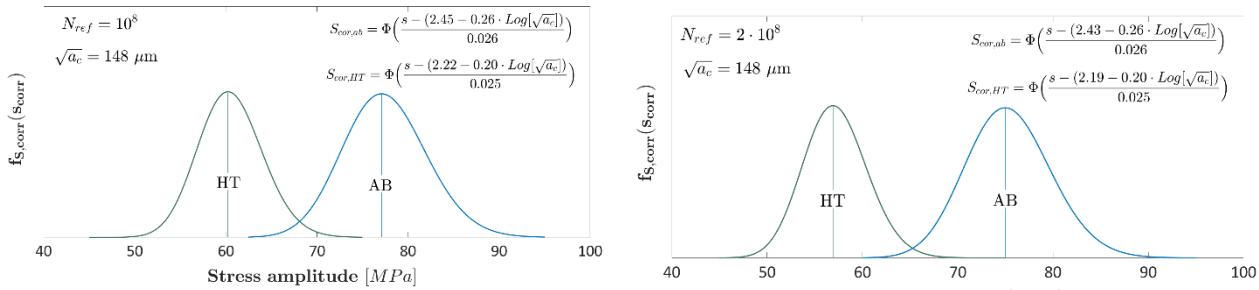

Figure 10: Probability density function of S_{corr} at: a) $n_{ref} = 10^8$ cycles; b) $n_{ref} = 2 \cdot 10^8$

Fig. 10 confirms that the tested heat treatment is detrimental for the VHCF response: if the median value is taken into account, the reduction is about 22% for $n_{ref} = 10^8$ cycles and 24% for $n_{ref} = 2 \cdot 10^8$ cycles. A hypothesis tests was also performed to verify if the VHCF strength of the HT specimens is statistically significantly different from the VHCF strength of the AB specimens. The P-value associated with the test was found to be close to 0 for both $n_{ref} = 10^8$ and $n_{ref} = 2 \cdot 10^8$. Therefore, by considering a significance level of 0.01, the null hypothesis was rejected. The hypothesis test further confirms that the investigated heat treatment cannot be employed for parts subjected to VHCF applications and the heat treatment parameters, such as the heating temperature, should be properly optimized.

In the following Section the factors (microstructural changes, residual stresses) involved in the reduction of the VHCF response will be investigated and discussed.

3.6. Discussion

The microstructural changes due to the heat treatment induce a significant reduction of the Vickers hardness, but an increment of the material ductility, which also affects the fatigue behavior of AM parts [10]. However,

the reduction of the Vickers hardness seems to have a larger influence on the VHCF response. In order to quantify the effect of the Vickers hardness on the VHCF response, the SIF threshold can be analyzed. According to Fig. 10, the SIF threshold trend is not affected by the heat treatment. By considering the model reported in [14] ($\Delta k_{th} = 3.3 \cdot 10^{-3} \cdot (HV + 120) \cdot \left(\sqrt{a_c}\right)^{1/3}$) or the general model in [44] ($k_{th} = c_{th} \cdot (HV + 120) \cdot \left(\sqrt{a_c}\right)^{1/2-\alpha_{th}}$), the ratio between the SIF threshold for AB specimens, $k_{th,AB}$, and for the HT specimens, $k_{th,HT}$, and the percentage difference, %Δ, become:

$$\frac{k_{th,AB}}{k_{th,HT}} = \frac{(HV_{AB}+120)}{(HV_{HT}+120)} \cong [87:73]\% \rightarrow \%\Delta \cong [13:27]\% \quad (2)$$

being HV_{AB} and HV_{HT} the Vickers hardness measured on AB and on HT specimens, respectively. The percent range in Equation 2 was estimated by considering the largest and the smallest HV_{AB} and HV_{HT}. The difference found in terms of median S_{corr} value was within the range computed in Equation 2 for the Vickers Hardness. Therefore, it can be argued that the decrease of the Vickers hardness caused by the heat treatment is the most responsible for the significant reduction of the VHCF response, with other factors, such as residual stresses and material ductility, having a negligible influence. The microstructural changes induced by the heat treatment (growth of large silicon particles after the rupture of the continuous silicon network) are detrimental for the VHCF response, even if the material ductility is significantly increased and the residual stresses are relieved. Experimental results highlighted the need for an optimization of the heat treatment in order to avoid microstructural changes which negatively affect the VHCF response and may thus limit the use of AM parts in structural applications.

The heat treatment was proposed with the aim of relieving residual stresses, which can be very high in as-built SLM parts. However, specimens were produced by heating the building platform up to 150° C (Table 2), which is an effective methodology for reducing residual stresses during the AM process, according to [11]. In particular, according to [11], residual stresses measured on specimens produced by heating the building platform are in the range $[6:10]$ MPa, whereas they slightly reduce after a subsequent stress relieve heat treatment ($[4:6]$ MPa). Experimental results confirmed that heating the building platform effectively limited

the residual stresses, even in AB specimens. The subsequent heat treatment further reduced the residual stresses, but with no significant effect on the fatigue response.

According to the above analysis, it can be concluded that the suggested heat treatment should be properly optimized to be employed in components used for applications where a large VHCF strength is required.

4. CONCLUSIONS

In the present paper, ultrasonic Very-High-Cycle Fatigue (VHCF) tests on AlSi10Mg alloy specimens produced through Selective Laser Melting (SLM) process were carried out. Fully reversed tension-compression tests were carried out on Gaussian specimens with a large risk-volume of $2300\ \mathrm{mm}^3$. The aim of the paper was to investigate the effect of a conventional stress relief heat treatment on the VHCF response. Experimental tests were carried out on as-built specimens and specimens subjected to the suggested stress relief heat treatment. Before the experimental tests, specimens were finely polished, in order to enhance the probability of crack nucleation from internal defects and investigate the influence of defect population on the VHCF response.

Quasi-static mechanical properties were at first compared. The tensile strength significantly decreased after the heat treatment, being about one half of the as-built specimens, whereas the ductility significantly increased, being about 2.4 times that of the as-built specimens. As for the tensile strength, the Vickers hardness significantly decreased after the heat treatment, from $134\ \mathrm{HV}$ to $76\ \mathrm{HV}$. The reason for this significant reduction was related to microstructural changes induced by the selected heating temperature. Indeed, the rupture and spheroidization of the continuous Si network, together with the coarsening of coherent β precipitates, made dislocation glide easier, thus lowering the mechanical response.

VHCF tests were carried out up to failure or to 10^9 cycles (runout specimens). All VHCF failures originated from superficial and sub-superficial defects in both as-built and heat treated specimens. Spherical pores were found to be the most critical defects, being at the origin of the fatigue failure in almost all specimens (67% in as-built and 80% heat treated). The pore size was not influenced by the heat treatment: the size range was found to be similar in as-built and heat treated specimens. Other less frequent defects were also found

in as-built and heat treated specimens: incomplete fusions and defects originating during the removal of support structures.

The VHCF response was finally compared: for the same number of cycles to failures, VHCF failures in as-built specimens occurred at larger stress amplitude. By comparing the VHCF strength at 10^8 and $2 \cdot 10^8$ cycles, the median value for the as-built specimens was about 20% larger than that for the heat treated specimens. Experimental results showed that the decrease of the Vickers hardness was the most responsible for the significant reduction of the VHCF response, with other factors, such as the residual stresses and the material ductility, having a negligible effect. Residual stresses were found to have a limited influence on the VHCF response, since specimens were produced by heating the building platform.

To conclude, experimental results highlighted that heat treatments should be carefully optimized to enhance the mechanical properties and, in particular, the VHCF response of SLM parts. Indeed, even if the process parameters are properly chosen and permit to manufacture parts characterized by acceptable fatigue and VHCF properties, the effect of an improper heat treatment could be significantly negative. The tested heat treatment should be optimized (e.g., by varying the heating temperature and the heating time) to avoid the microstructural changes which were shown to be detrimental for the VHCF response. Moreover, experimental results further confirmed that a proper experimental characterization is necessary to further extend the use of AM parts in critical structural applications where a reliable VHCF response is required.

ACKNOLEDGMENTS

The Authors acknowledge the Piedmont Region Industrial Research Project STAMP (Sviluppo Tecnologico dell'Additive Manufacturing in Piemonte, MIUR – POR FESR 2014/2020 – Azione 3 Piattaforma Tecnologica "Fabbrica Intelligente") and Accordo Quadro CNR/Regione Lombardia n. 3866 del 17/07/2015 FHfFC for financial support, Beam It for technical assistance.

REFERENCES

[1] Kempen K, Thijs L, Van Humbeeck J, Kruth JP. Processing AlSi10Mg by selective laser melting: parameter optimisation and material characterization. Mater Sc. Tech Ser 2015; 31:8: 917-923.

[2] Brandl E, Heckenberge U, Holzinger V, Buchbinder D. Additive manufactured AlSi10Mg samples using Selective Laser Melting (SLM): Microstructure, high cycle fatigue, and fracture behaviour. Mater Design 2012; 34: 159–169.

[3] Mower TM, Long MJ. Mechanical behavior of additive manufactured, powder-bed laser-fused materials, Mater Sci Eng A 2016; 651: 198–213.

[4] Uzan NE, Shneck R, Yeheskel O, Frage N. Fatigue of AlSi10Mg specimens fabricated by additive manufacturing selective laser melting (AM-SLM). Mater Sci Eng A 2017; 704: 229–237.

[5] Beretta S, Romano S. A comparison of fatigue strength sensitivity to defects for materials manufactured by AM or traditional processes. Int J Fatigue 2017; 94: 178-191.

[6] Wycisk E, Siddique S, Herzog D, Walther F, Emmelmann C. Fatigue Performance of Laser Additive Manufactured Ti–6Al–4V in Very High Cycle Fatigue Regime up to 10^9 Cycles Frontiers in Materials 2015; 2 (72): 1-8. doi.org/10.3389/fmats.2015.00072.

[7] Siddique S, Imran M, Walther F. Very high cycle fatigue and fatigue crack propagation behavior of selective laser melted AlSi12 alloy. Int J Fatigue 2017; 94: 246-254.

[8] Günther J, Krewerth D, Lippmann T, Leuders S, Tröster T, Weidner A, Biermann H, Niendorf T. Fatigue life of additively manufactured Ti–6Al–4V in the very high cycle fatigue regime. Int J Fatigue 2017; (94) Part 2: 236-245.

[9] Tridello A, Biffi CA, Fiocchi J, Bassani P, Chiandussi G, Rossetto M, Tuissi A, Paolino DS. VHCF response of as-built SLM AlSi10Mg specimens with large loaded volume. Fatigue Fract Engng Mate. Struct 2018; 41: 1918–1928.

[10] Aboulkhair NT, Maskery I, Tuck C, Ashcroft I, Everitt NM. Improving the fatigue behaviour of a selectively laser melted aluminium alloy: Influence of heat treatment and surface quality. Mater Design 2016; 104: 174–182.

[11] Siddique S, Imran M, Wycisk E, Emmelmann C, Walther F. Influence of process-induced microstructure and imperfections on mechanical properties of AlSi12 processed by selective laser melting. J Mater Process Technol 2015; 221: 205–213.

[12] Maskery I, Aboulkhair NT, Tuck C, Wildman RD, Ashcroft IA, Everitt NM, Hague RJM. Fatigue performance enhancement of selectively laser melted aluminium alloy by heat treatment. Proceedings of the 26th Solid freeform fabrication symposium (2015), Austin (USA), 1017-1025.

[13] Paolino DS, Rossetto M, Chiandussi G, Tridello A. Sviluppo di una macchina a ultrasuoni per prove di fatica gigaciclica, Proceedings of the 41th AIAS Conference (2012), Vicenza, (In Italian).

[14] Murakami Y. Metal Fatigue: Effects Of Small Defects And Nonmetallic Inclusions. 1st ed. Oxford: Elsevier Ltd; 2002.

[15] Furuya Y. Notable size effects on very high cycle fatigue properties of high strength steel. Mater Sci Eng A 2011; 528: 5234–5240.

[16] Paolino DS, Tridello A, Chiandussi G, Rossetto M. On specimen design for size effect evaluation in ultrasonic gigacycle fatigue testing. Fatigue Fract Engng Mater Struct 2014; 37: 570–579.

[17] Tridello A, Paolino DS, Chiandussi G, Rossetto M. VHCF response of AISI H13 steel: assessment of size effects through Gaussian specimens. Procedia Eng. 2015; 109: 121–127.

[18] Tridello A. VHCF response of Gaussian specimens made of high-strength steels: comparison between unrefined and refined AISI H13, Fatigue Fract Engng Mater Struct 2017; 40 (Issue 10): 1676–1689.

[19] Tridello A, Paolino DS, Chiandussi G, Rossetto M. VHCF strength decrement in large H13 steel specimens subjected to ESR process. Procedia Structural Integrity 2016; 2: 1117–1124. https://doi.org/10.1016/j.prostr.2016.06.143

[20] Tridello A, Paolino DS, Chiandussi G, Rossetto M. Effect of electroslag remelting on the VHCF response of an AISI H13 steel. Fatigue Fract. Engng. Mater. Struct. 2017; 40 (Issue 11): 1783–1794. https://doi.org/10.1111/ffe.12696

[21] Tridello A, Paolino DS, Chiandussi G, Rossetto M. Analytical design of gigacycle fatigue specimens for size effect evaluation. Key Eng. Mater. 2014; 577-558: 369-372. https://doi.org/10.4028/www.scientific.net/KEM.577-578.369

[22] SLM Solutions Group AG, 3D metals: the range of our standard metal powders (2018), Lubeck.

[23] ISO/ASTM 52921:2013 (2013) Standard terminology for additive manufacturing -- Coordinate systems and test methodologies. International Standard Organization (ISO), Genève.

[24] Renishaw plc, Laser Meting: Aluminum AlSi10Mg_25mm_AM250-400W Parameter Validation, 2014.

[25] Fiocchi J, Tuissi A, Bassani P, Biffi CA. Low temperature annealing dedicated to AlSi10Mg selective laser melting products. Journal of Alloys and Compounds 2017; 695:3402-3409.

[26] Biffi CA, Fiocchi J, Bassani P, Paolino DS, Tridello A, Chiandussi G, Rossetto M, Tuissi A. Microstructure and preliminary fatigue analysis on AlSi10Mg samples manufactured by SLM. Procedia Structural Integrity 2017; 7: 50-57.

[27] EN ISO 6507-1 (2005) Metallic materials - Vickers hardness test - Part 1: Test method, International Standard Organization (ISO), Genève.

[28] Tridello A, Paolino DS, Chiandussi G, Rossetto M. Comparison between dog-bone and Gaussian specimens for size effect evaluation in gigacycle fatigue. Frattura e Integrità Strutturale 2013; 26: 49-56.

[29] Bathias C, Paris PC. Gigacycle Fatigue in Mechanical Practice, 1st ed. New York: CRC Dekker; 2004.

[30] Tridello A, Paolino DS, Chiandussi G, Goglio L. An innovative testing technique for assessing the VHCF response of adhesively bonded joints. Fatigue Fract Engng Mater Struct 2019; 42: 84–96.

[31] Tridello A, Paolino DS, Chiandussi G, Rossetto M. Gaussian specimens for VHCF tests: Analytical prediction of damping effects Int J Fatigue 2016; 83: 36-41.

[32] Tridello A, Paolino DS, Chiandussi G, Rossetto M. Gaussian Specimens for Gigacycle Fatigue Tests: Evaluation of Temperature Increment Key Eng Mater 2015; 625: 85–88.

[33] Zhang J, Song B, Wei Q, Bourell D, Shi Y. A review of selective laser melting of aluminum alloys : Processing, microstructure, property and developing trends. J. Mater. Sci. Technol. 2019; 35: 270–284. doi:10.1016/j.jmst.2018.09.004.

[34] Aboulkhair NT, Maskery I, Tuck C, Ashcroft I, Everitt NM. The microstructure and mechanical properties of selectively laser melted AlSi10Mg: The effect of a conventional T6-like heat treatment, Mater Sci Eng A 2016; 667: 139–146. doi:10.1016/j.msea.2016.04.092.

[35] Li XP, Wang XJ, Saunders M, Suvorova A, Zhang LC, Liu YJ, Fang MH, Huang ZH, Sercombe TB. A selective laser melting and solution heat treatment refined Al – 12Si alloy with a controllable ultrafine eutectic microstructure and 25 % tensile ductility Acta Mater. 2015; 95: 74–82. doi:10.1016/j.actamat.2015.05.017.

[36] Calignano F. Design optimization of supports for overhanging structures in aluminum and titanium alloys by selective laser melting. J Mater 2014; 64: 203–213. doi:10.1016/j.matdes.2014.07.043.

[37] Yamashita Y, Murakami T, Mihara R, Okada M, Murakami Y. Defect Analysis and Fatigue Design Basis for Ni-based Superalloy 718 manufactured by Additive Manufacturing. Procedia Structural Integrity 2017; 7: 11-18.

[38] Girelli L, Tocci M, Montesano L, Gelfi M, Pola A. Optimization of heat treatment parameters for additive manufacturing and gravity casting AlSi10Mg alloy. IOP Conf. Ser. Mater. Sci. Eng. 2017; 264: 1-8. doi:10.1088/1757-899X/264/1/012016

[39] Girelli L, Tocci M, Gelfi M, Pola A. Study of heat treatment parameters for additively manufactured AlSi10Mg in comparison with corresponding cast alloy. Mater Sci Eng A 2019; 739: 317–328.

[40] Yang KV, Rometsch P, Davies CHJ, Huang A, Wu X. Effect of heat treatment on the microstructure and anisotropy in mechanical properties of A357 alloy produced by selective laser melting. Mater. Des. 2018; 154: 275–290.

[41] Maskery I, Aboulkhair NT, Corfield MR, Tuck C, Clare AT, Leach RK, Wildman RD, Ashcroft IA, Hague RJM. Quantification and characterisation of porosity in selectively laser melted Al-Si10-Mg using X-ray computed tomography. Mater Charact 2016; 111: 193–204.

[42] Romano S, Brückner-Foit A, Brandão A, Gumpinger J, Ghidini T, Beretta S. Fatigue properties of AlSi10Mg obtained by additive manufacturing: Defect-based modelling and prediction of fatigue strength. Eng Fract Mech. 2018; 187: 165-189.

[43] Matsunaga H, Sun C, Hong Y, Murakami Y. Dominant factors for very-high-cycle fatigue of high-strength steels and a new design method for components. Fatigue Fract Engng Mater Struct 2015; 38: 1274–1284.

[44] Paolino DS, Tridello A, Chiandussi G, Rossetto M. S-N curves in the very-high-cycle fatigue regime: statistical modeling based on the hydrogen embrittlement consideration. Fatigue Fract Eng Mater Struct 2016; 39: 1319-1336.

[45] Tridello A, Paolino DS, Chiandussi G, Rossetto M. Ultrasonic VHCF tests on AISI H13 steel with two different inclusion content: assessment of size effects with Gaussian specimens. Proceedings of the 7th Conference on Very High Cycle Fatigue, VHCF 7 (2017), Dresden (Germany).